Multiplicity of atomic reconfigurations in an electrochemical Pb single-atom transistor

F.-Q. Xie,[1,*] X.-H. Lin,[2] A. Gross,[2] F. Evers,[3] F. Pauly,[4] and Th. Schimmel[1,5,6,†]
[1]*Institute of Applied Physics, Karlsruhe Institute of Technology, Campus South, D-76128 Karlsruhe, Germany*
[2]*Institute of Theoretical Chemistry, Ulm University, D-89069 Ulm, Germany*
[3]*Institute I-Theoretical Physics, University of Regensburg, D-93040 Regensburg, Germany*
[4]*Department of Physics, University of Konstanz, D-78464 Konstanz, Germany*
[5]*Institute of Nanotechnology, Karlsruhe Institute of Technology, Campus North, D-76021 Karlsruhe, Germany*
[6]*Herbert Gleiter Institute of Nanoscience, Nanjing University of Science and Technology, 210094 Nanjing, China*
(Received 23 December 2016; revised manuscript received 12 April 2017; published 15 May 2017)

One focus of nanoelectronics research is to exploit the physical limits in size and energy efficiency. Here, we demonstrate a device in the form of a fully metallic atomic-scale transistor based on a lead (Pb) single-atom quantum point contact. The atomic configuration of the point contact determines the conductance of the Pb atomic-scale transistor. The conductance multiplicity of the Pb single-atom transistor has been confirmed by performing switching between an electrically nonconducting "off-state" and conducting "on-states" at $1G_0$($G_0 = 2e^2/h$, where e is the electron charge, and h Planck's constant), 2.0 G_0, 3.0 G_0, 1.5 G_0, 2.4 G_0, 2.7 G_0, 2.8 G_0, and 5.4 G_0, respectively. Our density-functional calculations for various ideal Pb single-atom contacts explain the atomic-configuration-related conductance multiplicity of the Pb single-atom transistor. The performance of the Pb single-atom transistors indicates that both the signatures of atomic valence and conductance quantization play roles in electron transport and bistable reconfiguration. The bistable reconfiguration of the electrode tips is an underlying mechanism in the switching of the Pb atomic-scale transistors. The absolute value of the electrochemical potential applied to the gate electrode is less than 30 mV. This merit suggests Pb [besides silver (Ag)] atomic-scale transistors as potential candidates for the development of electronic circuits with low power consumption. The dimension of the switching unit in the Pb single-atom transistor is in the range of 1 nm, which is much smaller than the projected scaling limit of the gate lengths in silicon transistors (5 nm). Therefore, the metallic single-atom transistors may provide perspectives for electronic applications beyond silicon.

DOI: 10.1103/PhysRevB.95.195415

I. INTRODUCTION

The scaling limit of the gate lengths in silicon transistors is projected to be 5 nm [1]. Many efforts have been made to fabricate electronic switching devices with functional building blocks at the atomic scale [2–20]. Among these atomic-scale devices, the transistor based on a silver point contact can be operated electrochemically with a potential applied to the gate electrode [2,3,5]. The atomistic modeling of structure and conductance elucidates bistable point-contact reconstruction as the physics of the transistor operation. For the silver single-atom transistor, the central cluster comprises a single atom connecting the two electrodes and all atoms within a radius of 0.9 nm around this central bottleneck. Only the atoms in the central cluster move in the switching process during the transistor operation [21]. Silver has the ground-state configuration of $[Kr]4d^{10}5s^1$ and only one s-valence electron. Theoretical calculations indicate that the conductance of silver single-atom point contacts changes only a little by tilting and twinning the angles of the two electrode tips with respect to one another. Therefore, the silver single-atom transistor switches between a nonconducting off-state and an on-state only at nG_0 (with integer n). The Pb electronic ground-state configuration is $[Xe]4f^{14}5d^{10}6s^26p^2$. Since the outermost d electrons are nearly 10 eV below the $6s$ band and approximately 20 eV below the Fermi level, the $5d$ levels can be viewed as core levels, and the electronic properties of Pb are dominated by the $6s$ and $6p$ bands. Pb adatoms on a Pb (111) surface were observed with a scanning tunneling microscope (STM), and it was confirmed that the adatoms possess sp^3 hybrid atomic orbitals. These hybrid orbitals have a specific orientation, and the four lobes are naturally oriented in a tetrahedral fashion [22]. The Pb point contacts have been investigated theoretically and experimentally with techniques such as the STM, the mechanically controllable break junction (MCBJ), and the electrochemical method [23–33]. The theoretical analysis of transport within the DFT approach demonstrates that the conductance of Pb single-atom contacts depends crucially on the contact geometry [27]. The STM measurement illustrates that the conductance evolution depends on the contact site, for instance, on-top, bridge, or hollow (hcp and fcc) sites in the Pb lattice, and shows the importance of atomic configuration in the conductance of atomic junctions [32]. Here, we investigate the possibility of Pb as a working material for metallic atomic-scale transistors and their electrochemically controllable single-atom switching with bistabilities related to the atomic geometries of Pb single-atom point contacts.

II. EXPERIMENT

Our experiment was performed in an electrochemical cell, which was shielded in a cylindrical inert gas (Ar) chamber. Figure 1 shows the fabrication of a Pb atomic-scale transistor, analysis of surfaces, and the schematic model of a single-atom transistor. The electrolyte solution consisted of

*fangqing.xie@kit.edu
†thomas.schimmel@kit.edu

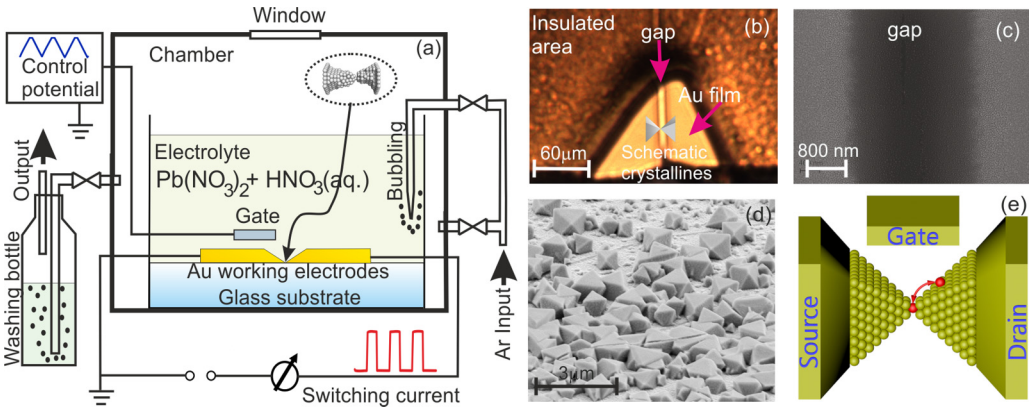

FIG. 1. Scheme of the experimental setup to fabricate Pb atomic-scale transistors, surface analysis, and the model of a single-atom transistor. (a) Pb is deposited and dissolved electrochemically in the narrow gap between two gold working electrodes on a glass substrate, and the conductance of the contact is measured simultaneously. The potentials of the working electrodes with respect to the lead reference electrode and the lead counter electrode are set by a potentiostat. (b) Confocal optical microscope image of as-prepared Au electrodes. The Au electrodes were insulated with a polymer film except for a shining triangle range for the electrochemical deposition of Pb. A schematic diagram of two Pb microcrystallines in gray is placed across the gap between the two gold electrodes to illustrate a point-contact formation. (c) Scanning electron microscopy image of a shadow-sputtered gap. (d) Scanning electron microscopy image of deposited Pb microcrystals on the Au electrodes. (e) Schematic model of a single-atom transistor.

1 mM $Pb(NO_3)_2$ + 0.1 M HNO_3 in bi-distilled water. Before starting electrochemical deposition, the chamber was flowed with Ar for 6 min. Then, the electrolyte was bubbled with Ar for around 2 h to expel oxygen in it. After these two steps, the chamber was flowed with Ar for another 3 min to take oxygen, which was expelled from the electrolyte, away from the chamber. With such kind of measure, an oxygen-free environment was created for the growth of lead atomic-scale point contacts. Two lead wires (0.5 mm diameter, 99.998% purity) were used as a counter electrode and a quasireference electrode. Two gold working electrodes were prepared on a glass substrate by shadow-sputtering under a carbon fiber of 5 μm in diameter, as shown in Fig. 1(a). The gold (Au) films of the working electrodes were approx. 100 nm thick. The working electrodes were covered with an insulating polymer coating except for the immediate contact area to minimize ionic conduction. Figure 1(b) shows the confocal optical microscope image of the as-prepared Au electrodes. The gap between two working electrodes was characterized by scanning electron microscopy, and we found a lot of Au islands in the shadow-sputtered range. Figure 1(c) shows a scanning electron microscopy image of a shadow-sputtered gap. One of the two working electrodes was virtually grounded. For conductance measurements, an additional potential of U_{bias} (−12.9 mV) was applied to the other working electrode. We changed only the potential of the reference electrode with respect to the ground. Therefore, the potential differences between the reference electrode and the two working electrodes were determined through U_{bias} and the reference-electrode potential, which was set by a computer-controlled bipotentiostat. Because the electrochemical current was in the range of nA, the potential difference between the reference electrode and counter electrode can be ignored in this case. We refer here to the combination of the reference electrode and counter electrode as the gate electrode. To fabricate an initial Pb contact in the gap between the two working electrodes, we applied a potential of 10–20 mV to the gate electrode. The Au islands in the shadow-sputtered range take the role of supporting Pb microcrystal deposition. While Pb islands were deposited in the gap, we monitored the conductance between the two working electrodes. Figure 1(d) displays a scanning electron microscopy image of deposited Pb microcrystals on the Au working electrodes. After the first junction formed between the two working electrodes, the deposition procedure continued for about 40 to 50 min. Such a kind of contact could survive in repeated opening-closing cycles for many days. After the initial stage, the contact was opened just by setting the gate-electrode potential in the range between −18 and −30 mV. The freshly opened junction was closed again by setting the gate-electrode potential between 5 and 18 mV. The gate electrode potential was changed in the deposition-dissolution cycling at the ramping rate of 50 mV/s. A schematic model of a Pb single-atom transistor is illustrated in Fig. 1(e).

In order to achieve conductance switching of Pb atomic-scale transistors, the potential applied to the gate was controlled via an analog-to-digital (A/D) card (National Instruments (NI) Peripheral Component Interconnect (PCI) 6221) by a program developed in the NI LabVIEW, and the conductance was recorded synchronously with the same program and card. The gate potential can be controlled either with a feedback mechanism or with a signal generation virtual instrument without the feedback mechanism, where the latter produces, for instance, constant, sine, triangle, and rectangular waves. The simultaneously recorded conductance and the electrochemical potential were sampled with the NI PCI 6221 at a rate of 50 1/s. For special high-resolution measurements, the conductance and the electrochemical potential were also recorded at the same time via a fast A/D card (NI PCI 6120) controlled by a home-made NI LabVIEW program installed on another computer. The sampling rate of the NI PCI 6120 was chosen to be 50 000 1/s. When the electrochemical potential was set using a feedback mechanism, the measured conductance was compared with a preselected value of quantum conductance of the Pb atomic-scale transistors. During the first such

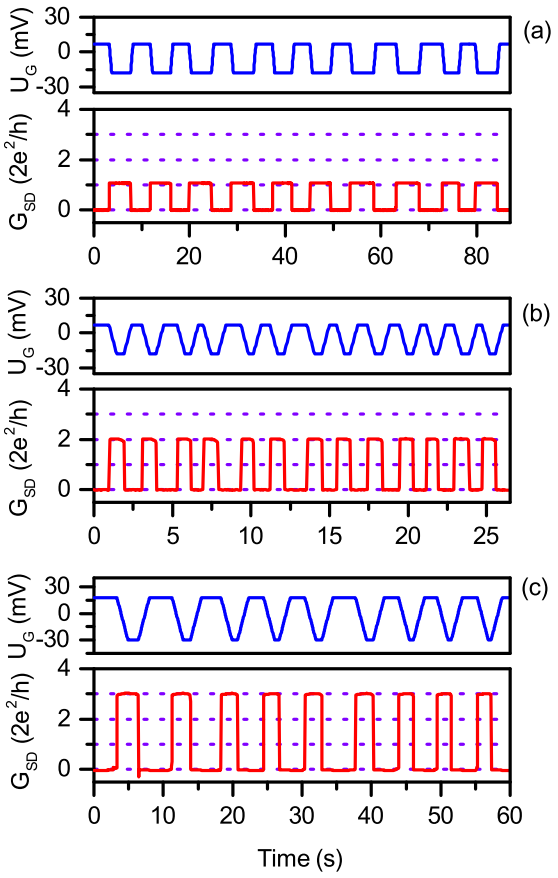

FIG. 2. Quantum conductance switching sequences of lead single-atom transistors. The transistors were controlled by an electrochemical potential applied to the gate electrode. By variation of the gate potential, a digital switching of the single-atom transistor was implemented between a nonconducting "off-state" and a quantized conducting "on-state" at (a) $1G_0$, (b) $2G_0$, and (c) $3G_0 (G_0 = 2e^2/h)$, respectively. The upper graph (blue) in each panel gives the electrochemical potential ("gate voltage") as a function of time, while the lower graph (red) is the simultaneously recorded source-drain conductance of the single-atom transistor on the same time scale.

dissolution-deposition cycles of each freshly formed contact, conductance values still varied from cycle to cycle. Only after repeated cycling, an abrupt change was observed from this irregular variation of the conductance values to a controlled and reproducible gate-voltage-induced switching between the two levels of 0 and a preselected value of quantum conductance in units of G_0. The fabrication and training procedure of the lead atomic-scale transistor is similar to our previously reported silver transistor.

III. RESULTS AND DISCUSSION

Figure 2 presents three examples of controlled switching between an electrically nonconducting "off-state" and conducting "on-states" with conductance values of $1G_0$ (a), $2G_0$ (b), and $3\,G_0$ (c) with $G_0 = 2e^2/h$. In Fig. 2, three sequences cut from longer ones of a few thousand switching events are illustrated to demonstrate conductance quantization of Pb single-atom transistors. The upper graphs (blue) of Figs. 2(a)–2(c) show the gate-electrode potential as a function of time, while the lower graphs (red) display the simultaneously recorded source-drain conductance of the single-atom transistor. Note that the corresponding transition of the contact conductance between the particular conducting on-state and the nonconducting off-state followed each of the transitions of the gate-electrode potential. Depending on the properties of the individual contacts, typical on/off ratios were more than 700.

Besides switching between an electrically nonconducting "off-state" and conducting "on-states" with integer quantum conductance at 1 G_0, 2 G_0, and 3 G_0, the lead single-atom transistor can implement operation between an "off-state" and "on-states" at 1.5 G_0, 2.3 G_0, 2.7 G_0, 2.8 G_0, and 5.4 G_0, respectively. The graphs of nine switching cycles for each "on-state" conductance are illustrated in the left column of Fig. 3, and the corresponding atomic contact geometries used for the charge transport calculations [27] are displayed in the right column. Our charge transport scheme is based on density-functional theory and the Landauer-Büttiker scattering theory [34]. The contact geometries used for the calculation of transport properties comprise a single-atom junction and a dimer junction for each of the main crystallographic directions ⟨100⟩, ⟨110⟩, and ⟨111⟩, where a single atom or a chain of two atoms form the connection between the electrodes. The single-atom and dimer contacts in the ⟨111⟩ direction have the same calculated values of conductance. Therefore, only one of the two geometries is shown in the right column of Fig. 3. The conductance is plotted on the same scale in the five graphs, while the axes of conductance are divided at different length units in each panel in order to plot adapted grid lines. Time axes are varied to meet the length of individual switching sequences. The possibility to realize multiple configurations with different conductance values of the lead single-atom transistor, i.e., their configurational multiplicity, is confirmed both experimentally and theoretically. The deposition-dissolution potentials are $5/-20$ mV (1.5 G_0), $15/-28$ mV (2.4 G_0), $16/-26$ mV (2.7 G_0), $18/-30$ mV (2.8 G_0), and $17/-26$ mV (5.4 G_0), respectively. The ramping rate of the electrochemical potential between deposition and dissolution is 50 mV/s. When the source-drain conductance was switched between the nonconducting "off-state" and the conducting "on-state" at 1.5 G_0, 2.4 G_0, 2.7 G_0, 2.8 G_0, and 5.4 G_0, respectively, almost only direct transitions were observed between these two states, and no intermediate levels were found during the switching process on the time scale shown in Fig. 3. This behavior is the same as that observed for the silver single-atom transistor. Thus, the results indicate that the switching transitions of the lead point contacts are also due to a reproducible, bistable atomic-scale reconfiguration. The switching between the nonconducting "off-state" and the conducting "on-state" at 1.5 G_0 was reproducibly operated for more than 12 h. The other switching processes, illustrated above, were shorter than this one.

In the preceding paragraphs, we used the term "single-atom" transistor for contacts that operate in the range of conductances up to around 5.3 G_0. This is the range of single-atom contact conductance values suggested by theory in Fig. 3. The direct transitions without intermediate states (that we will also discuss further below) provide further indirect evidence that the contacts are realized through single-atom

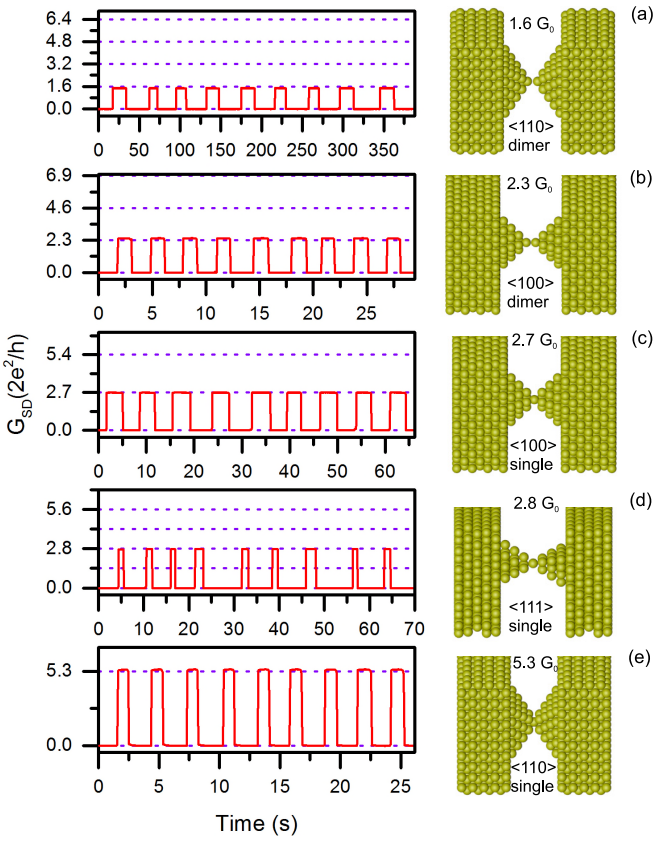

FIG. 3. Conductance multiplicity of the lead single-atom transistor. These graphs (left) illustrate that the Pb single-atom transistor can implement quantum conductance switching between an "off-state" and "on-state" at (a) 1.5 G_0, (b) 2.4 G_0, (c) 2.7 G_0, (d) 2.8 G_0, and (e) 5.4 G_0, respectively. The conductance is calculated using density-functional theory for various single-atom and dimer contacts oriented along the main crystallographic directions ⟨100⟩, ⟨110⟩, and ⟨111⟩ (right). The calculated conductance values are listed beside the atomic geometries. Because the dimer contact in the direction of ⟨111⟩ has the same conductance as its single-atom contact partner, its atomic configuration is not displayed here. Each graph shows nine switching cycles. The conductance is plotted on the same scale in the five graphs, while the axes of conductance are labeled in different length units in each panel for the convenience of plotting adapted grid lines. Time axes are scaled to meet the length of the individual switching sequences.

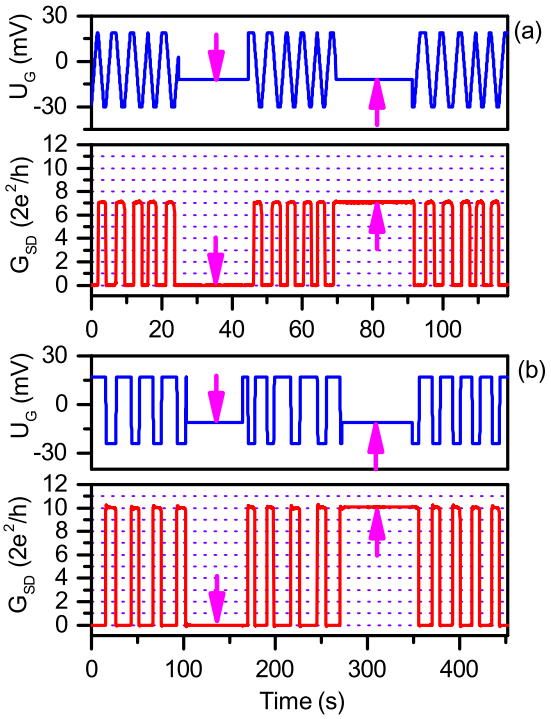

FIG. 4. Demonstration of switching and state-hold in two lead atomic-scale transistors. The transistors switched between the "off-state" and quantized "on-states." These on-states are (a) 7 G_0 and (b) 10 G_0. The quantum conductance switching (red) of the atomic-scale transistors, shown in panels (a) and (b), is directly controlled by the gate electrode potential (blue). These graphs also demonstrate that a conductance level can be kept stable if the gate potential is kept on a "hold" level (see arrows).

bridges. We will refer to transistors with on-state conductances above 5.3 G_0 as "multiatom" transistors.

By selection of the experimental parameters, the controlled reconfiguration of the Pb atomic-scale transistor, i.e., switching between zero and predefined higher conductance levels, was achieved. Figure 4 shows that two Pb atomic-scale transistors switched between the "off-state" and quantized "on-states" of 7 G_0 [Fig. 4(a)] and 10 G_0 [Fig. 4(b)], respectively. The quantum conductance switching (red) of these transistors was directly controlled by the gate-electrode potential (blue). The switching on/off potentials were 19/−29 mV [Fig. 4(a)], 17/−24 mV [Fig. 4(b)]. These graphs also demonstrate that a conductance level could be kept stable if the gate potential was set to a "hold" level (see arrows, −12 mV [Fig. 4(a)] and −11 mV [Fig. 4(b)]). As soon as the gate-electrode potential was set to the "hold" level, the present conductance state of the atomic-scale transistor remained stable and no further switching took place. At this holding potential, neither further electrochemical deposition nor dissolution of the contact was observed. Thus, the transistors can be operated reproducibly by the use of three values of the gate potential named *switching-on*, *switching-off*, and *hold*. By the ability to switch and keep the conductance, the Pb atomic-scale transistor provides perspectives for atomic-scale logical gates and atomic-scale digital electronics. The metallic atomic-scale transistors operate as resistive switches, which have been demonstrated to show volatile-nonvolatile dual functionality [2–5,18,20,35]. The transistors with volatile-nonvolatile dual functionality can be configured to perform a memory operation. Embedded nonvolatile memory could enable checkpointing (without the need to write to disk) and could offer the potential of instant-on processors. Such a merging of logic with memory might also open possibilities for processor-in-memory and logic-in-memory architectures [36]. There is certainly no shortage of new device concepts, but given the existing wide-scale expertise and infrastructure, the metallic atomic-scale transistors, at least in the short term, are likely to be those that can be integrated with conventional chip technology.

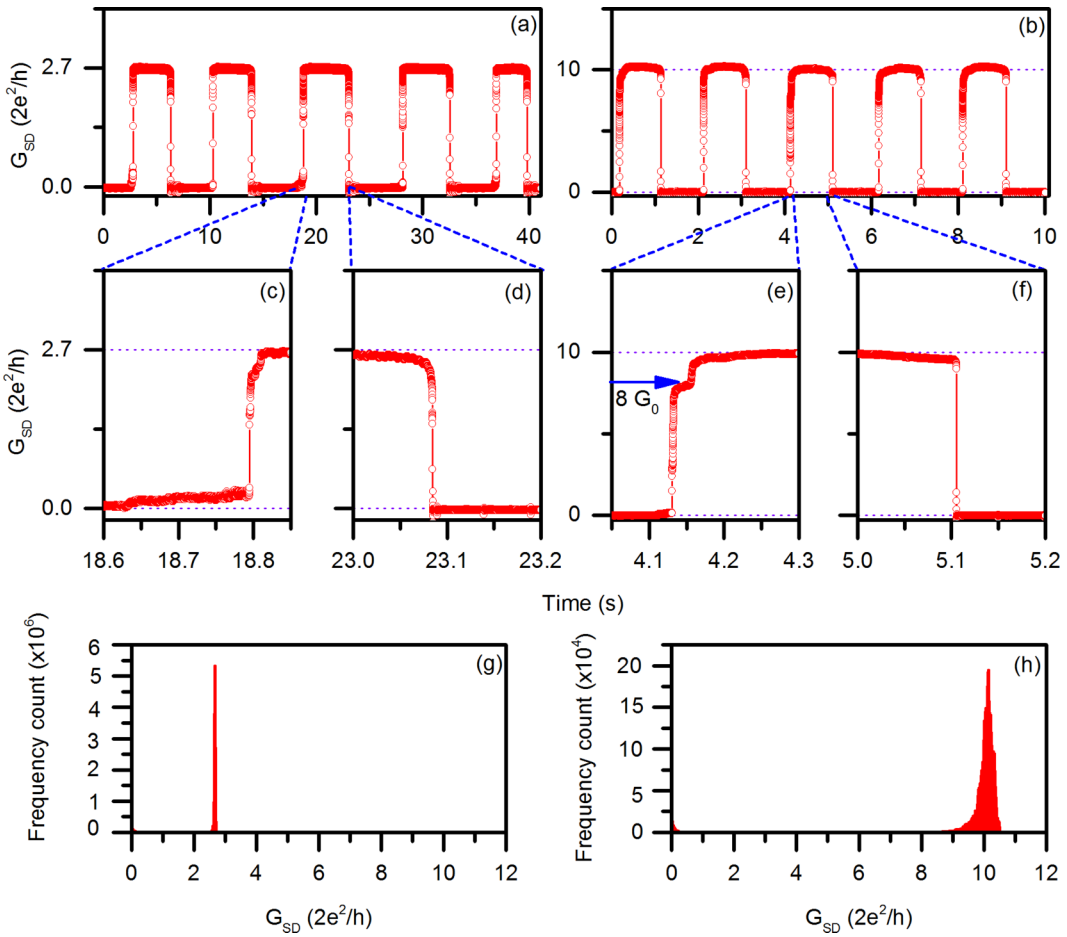

FIG. 5. Detailed comparison of two switching sequences, (a) 0–2.7 G_0 and (b) 0–10 G_0. The data of the two sequences was recorded at a sampling rate of 50 000 1/s. Graphs (a) and (b) show only five cycles for each switching, the small empty circles indicate measured data, and the lines are guidance for the eye. Graphs (c), (d), (e), and (f) display closing and opening events of the third cycle in each sequence, respectively. The conductance histogram for each switching sequence of 68 cycles in total is presented in (g) and (h), respectively. The full width at half maximum is 0.06 G_0 around 2.67 G_0, and 0.30 G_0 around 10.13 G_0. For the histograms, the fast-recorded conductance data was collected in bin sizes of 0.02 G_0.

In order to compare the switching behavior of single-atom and multiatom transistors, we sampled conductance data at a high rate. The fast-recorded conductance data of two switching sequences (with 68 cycles in total in each case) of 0–2.7 G_0 and 0–10 G_0 is shown in Fig. 5. Five cycles for each switching are displayed in Figs. 5(a) and 5(b) and the small empty circles indicate measured data, while the lines are there to guide the eye. Figures 5(c)–5(f) display closing (in 0.25 s) and opening (in 0.2 s) processes of the third cycle in each sequence, respectively. In Fig. 5(c), we see the conductance increasing from 0 to 0.28 G_0 in 0.2 s, jumping to 1.4 G_0 within 0.2 ms, and finally relaxing from 1.4 G_0 to 2.7 G_0 in 0.015 s. In the opening procedure in Fig. 5(d), the conductance decreases from 2.7 G_0 to 2.3 G_0 in 0.082 s and then jumps to open within 2 ms. For the case of 0–10 G_0 switching in Fig. 5(e), the contact increases its conductance from 0 to 0.16 G_0 in 0.03 s, jumps from 0.16 G_0 to 7.5 G_0 in 0.004 s, rises from 7.5 G_0 to 8.3 G_0 with a low slope in 0.02 s, and then transits from 8.3 G_0 to 10 G_0 in 0.03 s. In the opening procedure, the conductance decreases from 10 G_0 to 9.1 G_0 in 0.1 s and then jumps to open within 0.4 ms. Conductance histograms for the 68 switching cycles of each transistor, taken with the fast recording, are presented in Figs. 5(g) and 5(h). For the histograms, the conductance data was divided into bins with a size of 0.02 G_0. Sharp peaks are found at conductances of 2.67 G_0 and 10.15 G_0. The full width at half maximum (FWHM) is 0.06 G_0 at 2.67 G_0 and 0.30 G_0 at 10.15 G_0.

The plateau state in the switching event of the 0–10 G_0 transistor at around 8 G_0 [see Fig. 5(e)] indicates that such high-conductance switches correspond to multiatom contacts, offering intermediate states. No clear plateaus of this kind are found for the thinner 0–2.7 G_0 transistor, compatible with the notion of single-atom contacts. We attribute the fact that this contact does not reach its final conductance in the closing event immediately to a quick release of strain that is building up during the reconfiguration. The scatter of conductance values around the on-state conductance is also enhanced for the 0–10 G_0 switch, as compared to the 0–2.7 G_0 case. Let us also note that the plateau state at around 8 G_0 is not occurring in each switching event and is therefore not visible in the histogram in Fig. 5(h).

A conventional semiconductor transistor works with three electrodes: source, drain, and gate. We try to make our device most comparable with a conventional semiconductor

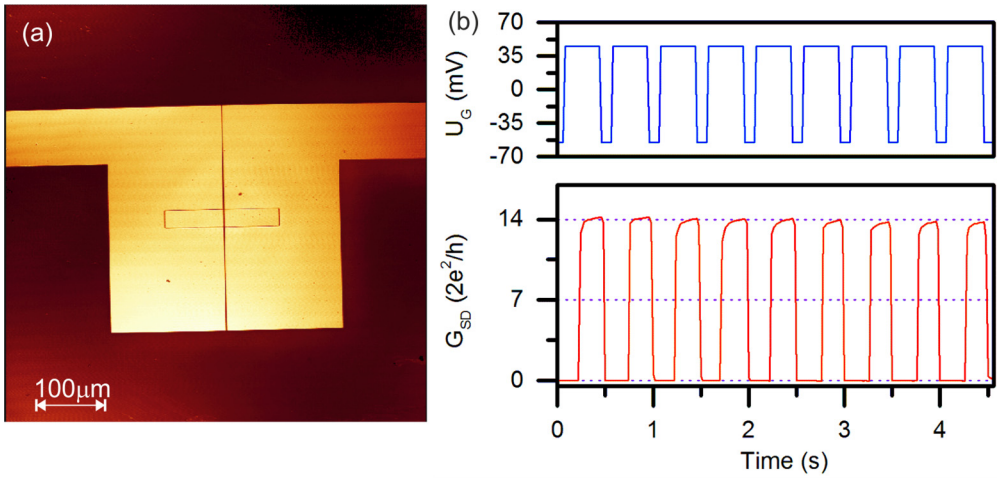

FIG. 6. Demonstration of rectangular-wave-driven switching of a Pb atomic-scale transistor between 0 and 14 G_0. The rectangular gate voltage wave was generated by an NI LabVIEW signal generation virtual instrument. The experiment was performed on a silicon wafer with a pair of Au electrodes separated by a gap of 2 μm and covered with a layer of photoresist SU-8 that is 2 μm thick. The optical microscope image is shown in panel (a). A rectangular window is opened in the SU-8 film over the Au electrodes with dimensions of 200 × 32 μm^2. The window is used for electrochemical deposition-dissolution. A point contact is formed across the gap in the window. In panel (b), the upper graph (blue) displays a rectangular switching sequence of the electrochemical potential applied to the gate electrode. The parameters characterizing the sequence are an amplitude of 50 mV with a shift of −5 mV (−55 mV to 45 mV), a frequency of 2 Hz, and a 75% duty cycle. The lower graph (red) shows the conductance switching between 0 and 14 G_0 following the rectangular wave of the electrochemical potential with a delay of around 0.17 s.

transistor. For this purpose, we use a pair of microelectrodes as source and drain. The microelectrodes (Cr/Au, 3 nm/40 nm thick), covered with an SU-8 photoresist film (2 μm) on a silicon wafer with a thin thermally oxidized SiO_2 film (300 nm), were fabricated by a standard photolithography method. The gap between the microelectrodes is 2 μm. The wafer with the SU-8 film was baked at 210 °C for 1 h to solidify the SU-8 film. Because the electrochemical current is less than 1 nA in our experiment, the use of the electrochemical reference electrode is not necessary. Only an electrochemical counter electrode (a Pb wire, 0.5 mm in diameter, 99.998% purity) is used here as a gate for the metallic atomic-scale transistor. A similar effort has been made for the operation of copper atomic-scale transistors [37]. The optical microscope image of the microelectrodes is shown in Fig. 6(a). A rectangular window is opened in the SU-8 film on the Au electrodes with dimensions of 200 × 32 μm^2. The window is used for electrochemical deposition-dissolution. A point-contact is formed cross the gap in the window. With the feedback mechanism, we realized a conductance switching between 0 and 14 G_0 and then switched the control of the gate potential from the feedback mechanism to a rectangular wave given by the signal generation virtual instrument. The signal generation virtual instrument drove the Pb atomic-scale transistor, implementing an operation between 0 and 14 G_0. In Fig. 6(b), the upper graph (in blue) displays a rectangular electrochemical potential wave applied on the gate electrode. The sequence (2 Hz, −55 mV to 45 mV, 75% duty cycle) was given by the virtual function generator in NI LabVIEW. The lower graph shows the conductance switching between 0 and 14 G_0, following the change of the electrochemical potential with a delay of around 0.17 s. The results show that our transistors can also be operated with three electrodes only and without the feedback mechanism.

The conductance of single-atom Pb contacts in ideal geometries was calculated to be 2.7 G_0, 5.3 G_0, and 2.8 G_0 for the main crystallographic orientations of the electrodes, namely, ⟨100⟩, ⟨110⟩, and ⟨111⟩, respectively. That of dimer Pb contacts in the ⟨100⟩, ⟨110⟩, and ⟨111⟩ orientations with ideal structures were predicted theoretically to be 2.3 G_0, 1.6 G_0, and 2.8 G_0, correspondingly [27]. The conductance histograms measured with the MCBJ technique at liquid helium temperatures and under cryogenic vacuum exhibit a broad peak between 0 and 3 G_0 [28,33,38]. The electrochemical method at room temperature and in the liquid solution has resolved the first broad peak in the conductance histogram of lead point contacts into sharp individual peaks at 1.0 G_0, 1.4 G_0, 2.0 G_0, 2.8 G_0, and 3.0 G_0 [27]. The conductance of metallic single-atom point contacts depends sensitively on the chemical valence of the atoms at the minimal cross section and their coupling to the neighboring atoms in both banks. Pb single-atom contacts exhibit 3 channels at the Fermi energy [27]. Scheer *et al.* showed that atomic contacts, which have nearly the same conductance (1.4 G_0), may have quite different transmission coefficients in all contributing channels [23]. By comparing the conductance histograms of lead atomic contacts, measured by the MCBJ technique and the electrochemical method, it is obvious that the conductance histogram depends not only on the metal's chemical valence but also on the preparation methods. Besides two noninteger conductance peaks at 1.4 G_0 and 2.8 G_0, three integer peaks were observed at 1 G_0, 2 G_0, and 3 G_0. Such kind of peaks at integer quantum conductance values have not been resolved in the conductance histogram measured with the MCBJ technique. The atomic contacts with integer quantum conductance at 1 G_0, 2 G_0, and 3 G_0 should not be in the ideal geometries. While conductance quantization might play a role, further explanations based on the electrochemical environment or the particular junction

setup cannot be excluded. The lead point contact has many possible nonideal atomic configurations just by tilting and twinning from the aforementioned ideal atomic configurations. Some of them may have electron transmission coefficients at integers. The interpretation of the peaks at integers of G_0 as a result of the conductance quantization of a free-electron gas in a geometrical constriction, as observed in semiconductor heterostructures [39,40] and *s*-type [41] metals, does not consider the complexity of electronic configurations in multivalent metal point contacts [27]. Additionally, absorption of molecules or ions on the lead point contacts in the electrolyte (e.g., O_2, H_2O, Ag^+, H^+, NO_3^-) may influence their electron transport. For instance, small molecular or ionic species could bridge the lead electrodes, or the contact might not be established between two Pb parts, as assumed in the theoretical calculations, but a Pb filament may contact the Au working electrodes or an Au cluster in the gap directly. It should furthermore be noted that the comparison of conductance histograms for Pb, generated with the MCBJ technique and the electrochemical method, requires some care. While conductance was sampled at a constant rate during the opening of the metallic contacts at a constant speed in the first case, conductance plateaus may be stable for a long time in the latter during the dissolution and deposition cycles [27]. All our identified peaks are enclosed in the first broad peaks illustrated in Refs. [33], [28], and [38]. They are therefore most likely related to single-atom contacts with different geometrical arrangements in both banks. Lead single-atom transistors can switch between "off-state" and "on-states" at 1.0 G_0, 1.5 G_0, 2.0 G_0, 2.4 G_0, 2.7 G_0, 2.8 G_0, 3.0 G_0, and 5.4 G_0, respectively. By comparing with the silver single-atom transistor [2], these results show the conductance multiplicity of lead single-atom transistors, offering a larger range of possible on-state conductances.

The silver and lead atomic-scale transistors were operated in almost the same electrochemical environment except for the metallic ions: The ion Ag^+ was replaced by the ion Pb^{2+}. The switching mechanism investigated for the silver atomic-scale transistors [21] can be applied to the lead atomic-scale ones, studied here. The change in the electrochemical potential induces a change in interface tension at the liquid-metal interface, leading to a deformation of the junction geometry parallel to the junction axis. The mechanical tension thus induces the switching process. The junction rips apart at some finite displacement from the equilibrium. For all junctions, this process is accompanied by a surface reorganization on at least one, but often both tips of the electrodes. By reversing the tension on the surface, executed by the electrochemical double layers, the surface reorganization is reversed with sub-Angstrom precision and the junction snaps into nearly the same atomistic conformation. The mass transport necessary for the reorganization of the lead electrode surface is facilitated by exchange diffusion processes, as demonstrated by density-functional theory calculations [30]. After some time of training, the junction geometries become increasingly stable and alternate between two bistable conformations by variation of the electrochemical potential applied to the gate electrode.

The observed reversible switching is explained by the generation of bistable contact geometries during the deposition cycle [2]. If we consider the tip atoms at each side of the electrodes in the open junction, the equilibrium geometry of both tips depends on their environment. In the open junction, this environment is defined by the remaining electrode atoms on one side. In the closed junction, the tip of the other electrode is also present. Reversible switching over many cycles is thus explained by reversible tip reorganization under the influence of the gate potential, similar to induced surface reorganization [42–45]. While the overall structure may differ between junctions with the same conductance value from one realization to the next, the minimal cross-section that determines the conductance is largely conserved.

The bistable reconfiguration of the electrode tips is another underlying mechanism of the formation of nanojunctions with predefined levels of quantum conductance. These levels are determined by the possible bistable junction conformations. Similar to magic numbers for metal clusters [42], those are most likely material specific. For silver, the observed quantum conductance levels coincide with integer multiples of the conductance quantum [2]. For lead point contacts, both conductance quantization and the chemical valence signatures appear to play roles in the determination of bistability. The Pb single-atom transistor can switch between an electrically nonconducting "off-state" and a conducting "on-state" with conductance not only at integer values of 1 G_0, 2 G_0, 3 G_0, but also at noninteger values of 1.5 G_0, 2.4 G_0 2.7 G_0 2.8 G_0, 5.3 G_0, respectively. By snapping into "magic" bistable conformations, junctions are mechanically and thermally stable at room temperature for long sequences of switching cycles, which offers interesting technological perspectives.

IV. SUMMARY

In summary, the metallic Pb atomic-scale transistor can operate in an electrochemical cell under Argon protection. Conductance multiplicity of the Pb single-atom transistor has been demonstrated by performing switching between an electrically nonconducting "off-state" and a conducting "on-state" at 1.0 G_0, 1.5 G_0, 2.4 G_0, 2.0 G_0, 2.7 G_0, 2.8 G_0, 3.0 G_0, and 5.4 G_0, respectively. The experimental noninteger values of quantum conductance are in good consistency with theoretical conductance calculations of ideal Pb atomic contact geometries [27]. The performance of the Pb single-atom transistor indicates that both the signatures of atomic valence and conductance quantization play a role in electron transport through its atomic contacts. By the theoretical calculations and high temporal resolution measurements of switching sequences, we believe that Pb point contacts have only one atom in the narrow connects, when their conductance is lower than or equal to 5.3 G_0. The lowest operation potentials for on/off switching were only 7 mV/-18 mV, respectively. The dynamic power dissipation of the complementary metal-oxide-semiconductor devices is proportional to the square of drain supply voltage (V_{DD}) [46]. The merit of the low operation potentials recommends the Pb atomic-scale transistor as a potential candidate for the development of electronic circuits with low power consumption. On the other hand, the Pb atomic-scale transistor operates at room temperature and allows high current input and output of the order of 1 μA, enabling high signal-to-noise ratios. At the same time, it is completely made of one and the same metal in the region of the

narrowest constriction. Limitations are presently set by slow switching rates due to capacitive effects in the electrochemical cells as well as the deposition-dissolution. The latter does not just take place locally at the narrowest constriction, where the switching occurs, but everywhere over the working electrodes. This might be improved by miniaturizing the electrochemical cells. In addition, lifetimes need to be improved, which are presently on the order of 14 000 switching cycles. The device with such low operation voltage can be applied to a standby electronic circuit with very low power consumption. We have demonstrated here that the Pb atomic-scale transistor can be set at "off," "on," and "hold" states, just by setting the gate potential at corresponding levels. This property provides the basis for atomic-scale logical gates and atomic-scale digital electronics. We have confirmed here that the Pb point contact is another good candidate for atomic-scale transistors besides silver.

ACKNOWLEDGMENTS

This work was supported by the Baden-Württemberg Foundation within the Network of Excellence Functional Nanostructures, the Carl-Zeiss Foundation, the Deutsche Forschungsgemeinschaft within the Center for Functional Nanostructures (CFN), and the Volkswagen-Stiftung.

[1] International Technology Roadmap for Semiconductors 2.0, 2015 edition, http://www.itrs2.net/itrs-reports.html.
[2] F. Q. Xie, L. Nittler, C. Obermair, and T. Schimmel, Phys. Rev. Lett. **93**, 128303 (2004).
[3] F. Q. Xie, C. Obermair, and T. Schimmel, Solid State Commun. **132**, 437 (2004).
[4] T. Hasegawa *et al.*, Appl. Phys. Express **4**, 015204 (2011).
[5] C. Obermair, F.-Q. Xie, and T. Schimmel, Europhys. News **41**, 25 (2010).
[6] J. Park *et al.*, Nature **417**, 722 (2002).
[7] W. J. Liang, M. P. Shores, M. Bockrath, J. R. Long, and H. Park, Nature **417**, 725 (2002).
[8] S. Kubatkin, A. Danilov, M. Hjort, J. Cornil, J. L. Bredas, N. Stuhr-Hansen, P. Hedegard, and T. Bjornholm, Nature **425**, 698 (2003).
[9] A. R. Champagne, A. N. Pasupathy, and D. C. Ralph, Nano Lett. **5**, 305 (2005).
[10] C. A. Martin, R. H. M. Smit, H. S. J. van der Zant, and J. M. van Ruitenbeek, Nano Lett. **9**, 2940 (2009).
[11] M. Fuechsle, J. A. Miwa, S. Mahapatra, H. Ryu, S. Lee, O. Warschkow, L. C. L. Hollenberg, G. Klimeck, and M. Y. Simmons, Nat. Nanotechnol. **7**, 242 (2012).
[12] D. P. E. Smith, Science **269**, 371 (1995).
[13] K. Terabe, T. Hasegawa, T. Nakayama, and M. Aono, Nature **433**, 47 (2005).
[14] C. Schirm, M. Matt, F. Pauly, J. C. Cuevas, P. Nielaba, and E. Scheer, Nat. Nanotechnol. **8**, 645 (2013).
[15] C. Obermair, M. Kress, A. Wagner, and T. Schimmel, Beilstein J. Nanotechnol. **3**, 824 (2012).
[16] C. Z. Li and N. J. Tao, Appl. Phys. Lett. **72**, 894 (1998).
[17] J. Z. Li, T. Kanzaki, K. Murakoshi, and Y. Nakato, Appl. Phys. Lett. **81**, 123 (2002).
[18] A. Sebastian, M. Le Gallo, and D. Krebs, Nat. Commun. **5**, 4314 (2014).
[19] I. Valov, E. Linn, S. Tappertzhofen, S. Schmelzer, J. van den Hurk, F. Lentz, and R. Waser, Nat. Commun. **4**, 1771 (2013).
[20] E. Mikheev, B. D. Hoskins, D. B. Strukov, and S. Stemmer, Nat. Commun. **5**, 3990 (2014).
[21] F. Q. Xie, R. Maul, A. Augenstein, C. Obermair, E. B. Starikov, G. Schoen, T. Schimmel, and W. Wenzel, Nano Lett. **8**, 4493 (2008).
[22] J. C. Lian *et al.*, Phys. Rev. B **81**, 195411 (2010).
[23] E. Scheer, N. Agrait, J. C. Cuevas, A. L. Yeyati, B. Ludoph, A. Martin-Rodero, G. R. Bollinger, J. M. van Ruitenbeek, and C. Urbina, Nature **394**, 154 (1998).
[24] J. C. Cuevas, A. L. Yeyati, and A. Martin-Rodero, Phys. Rev. Lett. **80**, 1066 (1998).
[25] N. Agrait, J. G. Rodrigo, and S. Vieira, Phys. Rev. B **47**, 12345 (1993).
[26] Z. Gai, X. W. Li, B. Gao, R. G. Zhao, W. S. Yang, and J. W. M. Frenken, Phys. Rev. B **58**, 2185 (1998).
[27] F. Q. Xie, F. Hueser, F. Pauly, C. Obermair, G. Schoen, and T. Schimmel, Phys. Rev. B **82**, 075417 (2010).
[28] P. Makk, S. Csonka, and A. Halbritter, Phys. Rev. B **78**, 045414 (2008).
[29] M. Becker and R. Berndt, New J. Phys. **12**, 113010 (2010).
[30] X. Lin, A. Dasgupta, F. Xie, T. Schimmel, F. Evers, and A. Gross, Electrochim. Acta **140**, 505 (2014).
[31] H. Kim and Y. Hasegawa, Phys. Rev. B **93**, 075409 (2016).
[32] H. Kim and Y. Hasegawa, Phys. Rev. Lett. **114**, 206801 (2015).
[33] A. I. Yanson, Dissertation, University Leiden, 2001.
[34] F. Pauly, J. K. Viljas, U. Huniar, M. Haefner, S. Wohlthat, M. Buerkle, J. C. Cuevas, and G. Schoen, New J. Phys. **10**, 125019 (2008).
[35] I. Valov and M. N. Kozicki, J. Phys. D: Appl. Phys. **46**, 074005 (2013).
[36] K. Bernstein, R. K. Cavin, III, W. Porod, A. Seabaugh, and J. Welser, Proc. IEEE **98**, 2169 (2010).
[37] F. Xie, M. N. Kavalenka, M. Röger, D. Albrecht, H. Hölscher, J. Leuthold, and T. Schimmel, Beilstein J. Nanotechnol. **8**, 530 (2017).
[38] J. G. Rodrigo and N. Agrait (Private communication).
[39] B. J. Vanwees, H. Vanhouten, C. W. J. Beenakker, J. G. Williamson, L. P. Kouwenhoven, D. Vandermarel, and C. T. Foxon, Phys. Rev. Lett. **60**, 848 (1988).
[40] D. A. Wharam *et al.*, J. Phys. C: Solid State Phys. **21**, L209 (1988).
[41] N. Agrait, A. L. Yeyati, and J. M. van Ruitenbeek, Phys. Rep. **377**, 81 (2003).
[42] M. N. Huda and A. K. Ray, Phys. Rev. A **67**, 013201 (2003).
[43] A. Ohiso, Y. Sugimoto, M. Abe, and S. Moritai, Jpn. J. Appl. Phys. **46**, 5582 (2007).
[44] P. Schnaebele, R. Korytar, A. Bagrets, T. Roman, T. Schimmel, A. Gross, and F. Evers, J. Phys. Chem. C **118**, 28252 (2014).
[45] M. Ternes, C. P. Lutz, C. F. Hirjibehedin, F. J. Giessibl, and A. J. Heinrich, Science **319**, 1066 (2008).
[46] L. Chang, D. J. Frank, R. K. Montoye, S. J. Koester, B. L. Ji, P. W. Coteus, R. H. Dennard, and W. Haensch, Proc. IEEE **98**, 215 (2010).